Fluctuation and Noise Letters
Vol. 12, No. 2 (2013) 1340007 (8 pages)

DOI: 10.1142/S0219477513400075

World Scientific
www.worldscientific.com

QUANTUM TRANSPORT IN BIOLOGICAL FUNCTIONAL UNITS: NOISE, DISORDER, STRUCTURE

T. ZECH*, M. WALSCHAERS†, T. SCHOLAK‡,
R. MULET§, T. WELLENS*,¶ and A. BUCHLEITNER*

*Physikalisches Institut, Hermann-Herder-Street 3
79104 Freiburg, Germany
¶Thomas.Wellens@physik.uni-freiburg.de

†Instituut voor Theoretische Fysica, KU Leuven
Celestijnenlaan 200D, B-3001 Heverlee, Belgium

‡Chemical Physics Theory Group, Department of Chemistry
University of Toronto, 80 St. George Street
Toronto, Ontario, M5S 3H6, Canada

§Complex System Group, Department of Theoretical Physics
University of Havana, Cuba

Received 14 November 2012
Accepted 27 May 2013
Published 15 July 2013

Communicated by Sandro Wimberger

Through simulations of quantum coherent transport on disordered molecular networks, we show that three dimensional structures characterized by centro-symmetric Hamiltonians exhibit on average higher transport efficiencies than random configurations. Furthermore, configurations that optimize constructive quantum interference from input to output site yield systematically shorter transfer times than classical transport induced by ambient dephasing noise.

Keywords: Transport processes; transport dynamics; biomolecules; structure and physical properties; quantum statistical methods; decoherence.

1. Introduction

Photosynthetic systems harvest solar energy with almost unit quantum efficiency However, recent experimental evidence of quantum coherence during the excitonic energy transport in photosynthetic organisms challenges our understanding of this fundamental biological function. In recent years, ultrafast optics and nonlinear spectroscopy experiments provided new insight into excitonic energy transport in photosynthetic organisms [1–4]. These experiments report the existence of long coherence

¶Corresponding author.

times, suggesting that quantum coherence may play a fundamental role in the highly efficient transport of excitations, and trigger renewed theoretical interest.

In our approach to the problem, we attempt to incorporate most of the documented properties of the electronic Hamiltonians that underlie excitonic transport in biological systems, and yet to outline a model as simple as possible [5, 6]. We therefore model light harvesting units as three-dimensional (3D) disordered networks, and study the corresponding statistics of the transport efficiency in Sec. 2. We will see that there exist certain optimal configurations of the network which achieve perfect population transfer of the excitation between predefined input and output sites. Concerning the structure of these configurations, we will unveil a statistical correlation between transfer efficiency and the degree of centro-symmetry of the underlying Hamiltonians in Sec. 3. Finally, the impact of dephasing noise will be studied in Sec. 4.

2. Model

Inspired by the structure of the FMO network — seven (FMO7) [7, 8] or eight (FMO8) [9] chromophores that are connected through dipolar interactions — we study the simplest possible random model which can grasp its essential ingredients: A small random network with N sites, where the coherent transport of a single excitation is generated by the Hamiltonian

$$H = \sum_{i \neq j = 1}^{N} V_{i,j} \sigma_+^{(j)} \sigma_-^{(i)}. \tag{1}$$

Here, $\sigma_+^{(j)}$ and $\sigma_-^{(i)}$ mediate excitations and de-excitations of sites j and i, from the local electronic ground state to the local excited state, and *vice versa*. The excitation transfer $\sigma_+^{(j)}\sigma_-^{(i)}$ from site i to site j has a strength $V_{i,j} = V_{j,i} = \alpha / r_{i,j}^3$, consistent with an isotropic dipolar interaction, with $r_{i,j} = |\vec{r}_i - \vec{r}_j|$, and the $\vec{r}_j$ the position vectors of individual sites. Input and output sites define the poles of a sphere of diameter d. The positions of the remaining molecular sites are randomly chosen within this sphere, which induces a random distribution of the remaining $V_{i,j}$. The excitation is initially injected at the input site $|\text{in}\rangle = |1\rangle$, from where it is to be transferred to the output site $|\text{out}\rangle = |N\rangle$. The coupling constant $V_{1,N} = \alpha / d^3$ between these two sites sets the natural time-scale of the dynamics induced by H. Since additional sites between input and output contribute to additional transition amplitudes, they tend to render the transport more efficient, in some analogy, e.g., to multiphoton excitation and ionization processes of atomic or molecular Rydberg states [10], or to the momentum spread of ultracold atoms under periodic forcing [11]. The intuition is that the additional sites, if properly placed, can mediate amplitudes which *interfere constructively* upon transmission, and thus ease the excitation transfer. A network will be considered *efficient* if the initial excitation is transferred to the output site in a time significantly smaller than the Rabi coupling

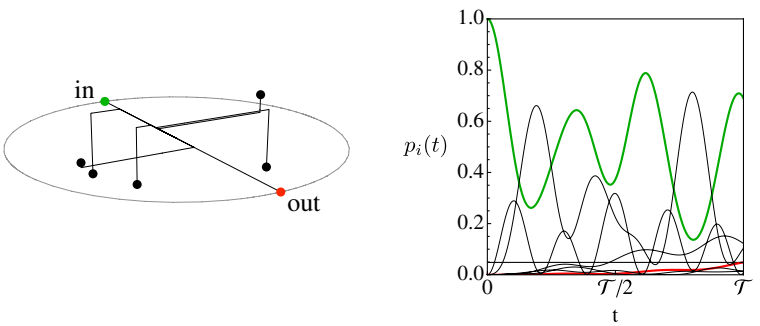

(a) (b)

Fig. 1. (Color online) (a) A typical configuration drawn from the random ensemble. The corresponding site positions are: $\vec{r}_1 = (-1, 0, 0)$, $\vec{r}_2 = (-0.76, -0.21, 0.43)$, $\vec{r}_3 = (-0.31, -0.10, 0.38)$, $\vec{r}_4 = (-0.25, 0.87, 0.41)$, $\vec{r}_5 = (-0.22, 0.78, -0.12)$, $\vec{r}_6 = (0.20, -0.70, -0.03)$, and $\vec{r}_7 = (1, 0, 0)$. The sites $|1\rangle = |\text{in}\rangle$ and $|7\rangle = |\text{out}\rangle$ are placed on the x-axis, whereas the y- (or z-) coordinates are represented by horizontal (or vertical) lines, (b) Time evolution of the occupation probabilities $p_i(t) = |\langle i| \exp(-iHt)|1\rangle|^2$ of the input site ($i = 1$, green), the output site ($i = 7$, red), and the intermediate sites ($i = 2, \ldots, 6$, black) for the Hamiltonian H defined by the spatial configuration shown in (a). The horizontal line indicates the transfer efficiency $\mathcal{P} = 0.048$ according to Eq. (2).

time $T = \pi/(2|V_{1,N}|)$ between $|\text{in}\rangle = |1\rangle$ and $|\text{out}\rangle = |N\rangle$, with high probability. For a quantitative assessment, we define the figure of merit [12, 13]

$$\mathcal{P} = \max_{t\in[0,\mathcal{T}]} |\langle N|e^{-iHt}|1\rangle|^2, \quad \mathcal{T} = 0.1 \times \pi/(2|V_{1,2}|). \tag{2}$$

A particular configuration is shown in Fig. 1(a) together with the probability $p_i(t) = |\langle i| \exp(-iHt)|1\rangle|^2$ of occupancy in each site during the coherent quantum dynamics. As can be seen in Fig. 1(b), the sample exhibits a rather low transfer efficiency, $\mathcal{P} = 0.048$. In Fig. 2, the distribution of transfer efficiencies is shown for

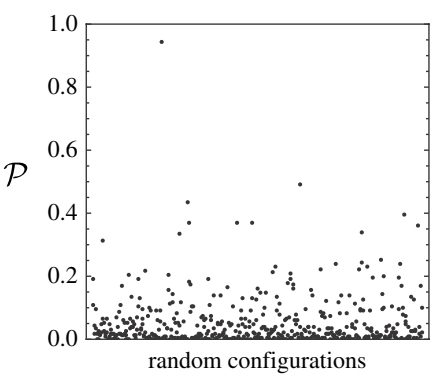

Fig. 2. Fluctuation of the transfer efficiency $\mathcal{P}$ from input to output, for 500 different random conformations of $N = 7$ sites. Most configurations provide very small efficiencies, but transport efficiencies up to 100% are also possible, though extremely rare.

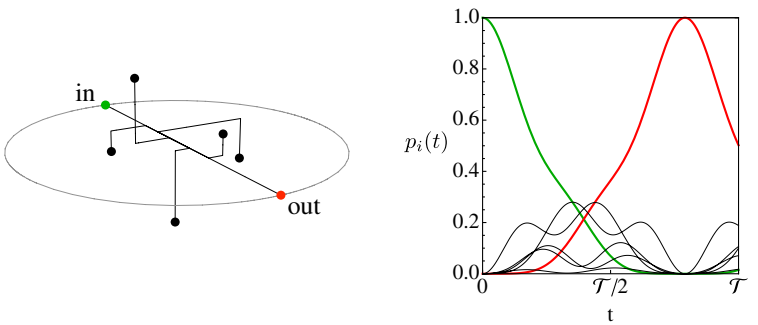

(a) (b)

Fig. 3. (Color online) (a) Optimal spatial configuration of $N = 7$ sites offering fast and perfectly lossless coherent transport from input to output. Site positions: $\vec{r}_1 = (-1, 0, 0)$, $\vec{r}_2 = (-0.39, -0.24, 0.13)$, $\vec{r}_3 = (-0.23, 0.63, 0.28)$, $\vec{r}_4 = (-0.09, -0.23, -0.39)$, $\vec{r}_5 = (0.15, -0.10, 0.44)$, $\vec{r}_6 = (0.35, 0.09, -0.13)$, $\vec{r}_7 = (1, 0, 0)$, (b) Time evolution of the on-site probabilites $p_i(t)$ generated by the Hamiltonian defined by (a). As in Fig. 1(b), i is either the input site ($i = 1$, green), the output node ($i = 7$, red), or an intermediate site ($i = 2, \ldots, 6$, black). At time $t \simeq 0.8\mathcal{T}$, only the output site is populated, leading to transfer efficiency $\mathcal{P} = 1$ according to Eq. (2). Note that the on-site probabilites are approximately time mirror-symmetric (with respect to $t \simeq 0.4\mathcal{T}$).

500 randomly chosen configurations. We see that low transfer efficiencies (of the order of only a few percent) – as for the configuration shown in Fig. 1(a) — are typical. However, there exist also configurations with high efficiency. Applying a genetic algorithm in order to maximize the transfer efficiency, we have checked that efficiencies $\mathcal{P} = 1$ can indeed be achieved [12]. An example of an optimized configuration realizing perfect excitonic population transfer ($\mathcal{P} = 1$) is shown in Fig. 3.

3. Optimal Configurations and Centrosymmetry

It is therefore important to understand what is common to these efficient configurations. A first hint comes from looking at the time evolution of the occupation probabilities of these structures. As can be observed in Fig. 3, the time evolution of the on-site probabilites $p_i(t)$ is essentially symmetric. In addition, one knows from previous works that centro-symmetric Hamiltonians are tunable towards perfect population transfer [14]. For the case of one-dimensional (1D) chains with nearest-neighbor coupling, the close connection between centro-symmetry and perfect state transfer has been explained in [15]. Moreover, a general mechanism for optimal transfer in disordered systems, with centro-symmetry as key ingredient, has recently been presented in [16].

Defining the deviation from the centro-symmetry by $\epsilon = \frac{1}{N} \min_S \|H - J^{-1}HJ\|$, where $\|A\| = [\mathrm{Tr}(A^\dagger A)]^{1/2}$ denotes the Hilbert–Schmidt norm, $J_{i,j} = \delta_{i,N-j+1}$ is the exchange matrix mapping the input and output sites 1 and N onto one another, and the minimum is taken over all permutations S of the intermediate sites

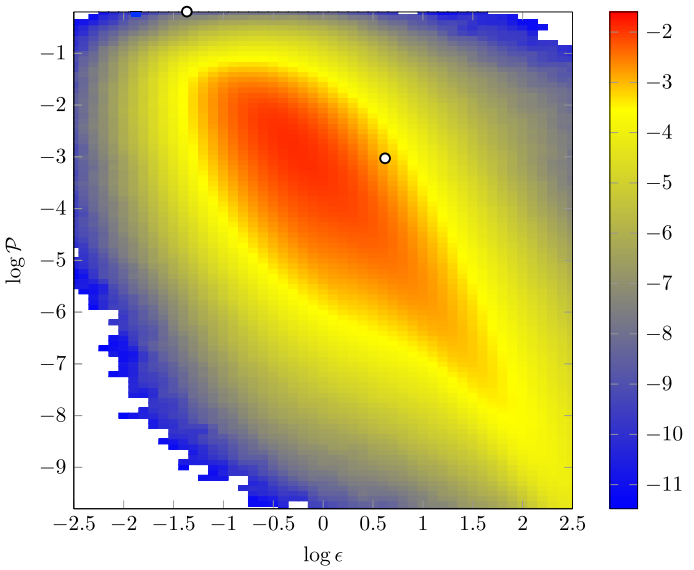

Fig. 4. (Color online) Correlation between efficiency $\mathcal{P}$ and centro-symmetry ϵ of 10^8 randomly generated 3D networks composed of $N = 7$ sites *in logarithmic* (*base e*) *scale*. The color code indicates the logarithm of the probability density of a pair $(\log(\epsilon), \log(\mathcal{P}))$. The two white circles represent the typical and the optimal configuration, respectively, from Figs. 1 and 3.

$2, \ldots, N-1$, we can show that in these systems there is a strong correlation between centro-symmetry and efficiency. Indeed, the optimal configuration shown in Fig. 3 exhibits a higher degree of centro-symmetry (i.e., smaller deviation from centro-symmetry $\epsilon = 0.253$) than the typical configuration shown in Fig. 1 ($\epsilon = 1.86$). For randomly chosen configurations, Fig. 4 shows the joint probability distribution of centro-symmetry and transfer efficiency. A clear correlation between ϵ and $\mathcal{P}$ is observed in Fig. 4, according to which higher values of the transfer efficiency $\mathcal{P}$ are associated with larger degrees of centro-symmetry (i.e., smaller values of ϵ), and *vice versa*.

4. Transfer Time and Noise

However, one must remember that the actual FMO complex *is* embedded in a noisy environment, and it therefore needs to be established whether the transport efficiency of the above, "optimal" conformations prevails in the presence of noise. We describe the underlying dynamics by the simplest possible model for open system evolution, incarnated by the master equation (where we set $\hbar = 1$, for convenience)

$$\dot{\varrho}(t) = -\mathrm{i}[H, \varrho(t)] - 4\gamma \sum_{i \neq j=1}^{7} |i\rangle\langle i|\varrho|j\rangle\langle j|. \tag{3}$$

Obviously, dephasing noise as modeled by Eq. (3) will disrupt destructive as well as constructive interference effects. The transfer efficiency of the "optimal" conformations will therefore be reduced by the noise, while the efficiency of the blocking conformations (those with low efficiencies, in the absence of noise) will increase.

In the actual FMO transport problem, the excitation is to be delivered irreversibly to a reaction center on output, which can be modeled by locally adding a decay term to the output site. This is implemented by adding a term

$$L_{\text{sink}}(\varrho) = \Gamma\left(|0\rangle\langle\text{out}|\varrho|\text{out}\rangle\langle 0| - \frac{1}{2}\{|\text{out}\rangle\langle\text{out}|, \varrho\}\right) \tag{4}$$

to the right-hand side of Eq. (3), where $|0\rangle$ and $\{,\}$ are the ground state of the molecular network and an anticommutator, respectively. The thus implied change of boundary conditions with respect to the closed system considered above also changes the geometry of those conformations which provide optimal transport

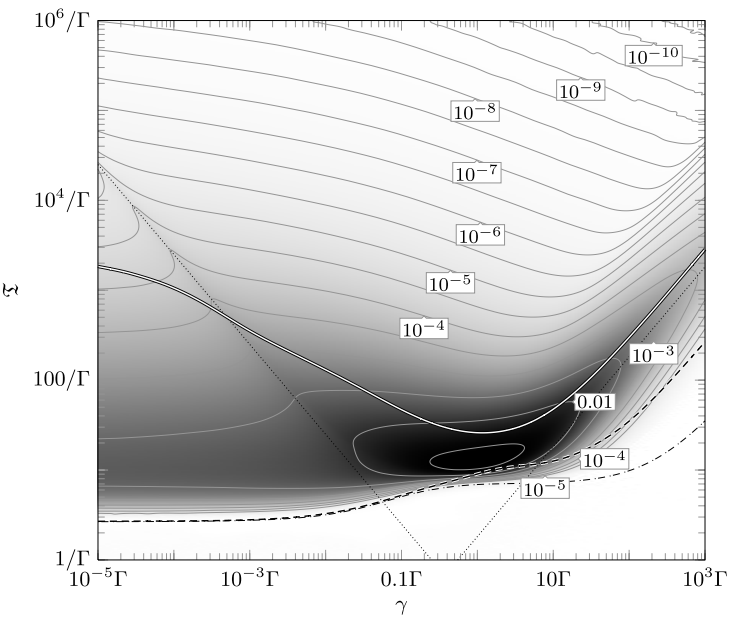

Fig. 5. (Color online) Probability density $f_{\mathfrak{T}}$ of the average excitation transfer time $\mathfrak{T}$, Eq. (5), for $N = 7$ molecular sites and sink rate $\Gamma = 10/T$, as a function of the dephasing rate γ [18]. The two dotted, diagonal lines are given by the dephasing time $\mathfrak{T}_{\text{deph}} = (4\gamma)^{-1}$, and by an approximate Zeno time $\mathfrak{T}_{\text{Zeno}} \propto \gamma$ (beyond which transport is "frozen", due to the Quantum Zeno projection mechanism), respectively. On time scales $\mathfrak{T} \gg \mathfrak{T}_{\text{deph}}$ (in the double-logarithmic plot), the purity of the excitonic state on the molecular network has dropped to its minimum value, hence the transport is essentially classical. The white line shows the median $\tilde{\mathfrak{T}}$, the dash-dotted line the minimum transfer time, and the dashed line the transfer time of a configuration that has been optimized for $\gamma = 0$. Clearly, this latter conformation achieves optimal transfer times over a broad range of dephasing rates, and in particular shorter than the optimal noise induced transfer times at $\gamma \simeq 1$.

efficiency, provided the sink coupling Γ is not too small [17]. However, the addition of a sink does not change the fundamental picture: Optimal transport efficiencies are achieved by those networks which define optimal coherent coupling between input and output site, and such coherence-induced optimal transport does always better than noise-induced excitation transfer. This is illustrated in Fig. 5 by a plot of the probability density of the excitation transfer time

$$\mathfrak{T} = \int_0^\infty (1 - \langle 0|\varrho(t)|0\rangle)\mathrm{d}t \tag{5}$$

(which is an alternative efficiency quantifier when the time scale for irreversible delivery of the excitation to the reaction center is to be quantified), as a function of the dephasing rate γ. Furthermore, since noise disrupts the system's specific interference properties, we see that it also blurs the distinction between different conformations.

5. Conclusion

The optimization landscape shown in Fig. 5 thus provides a clear picture of the possible strategies to achieve efficient transfer across a disordered quantum network: The large majority of randomly sampled configurations requires the *assistance of noise* to achieve efficient transport, which will occur on time scales clearly longer than the dephasing time, and therefore essentially be of classical nature. In contrast, Fig. 5 also shows that a small but finite sub-ensemble of *optimal configurations* mediates *efficient quantum transport* of the excitation from input to output, faster than the noise-assisted, classical transport.

Concerning the structure of these optimal configurations, we have shown that networks corresponding to Hamiltonians with *high degree of centro-symmetry* exhibit on average *higher transfer efficiencies* than those with less centro-symmetry. This result shows that what appears to be geometrically disordered complexes may well exhibit certain symmetries which enhance energy transport between chromophores.

References

[1] H. Lee, Y. C. Cheng and G. Fleming, Coherence dynamics in photosynthesis: Protein protection of excitonic coherence, *Science* **316** (2007) 1462–1465.

[2] G. Engel, T. R. Calhoun, E. L. Read, T.-K. Ahn, T. Mancal, Y. C. Cheng, R. E. Blankenship and G. Fleming, Evidence for wavelike energy transfer through quantum coherence in photosynthetic systems, *Nature* **446** (2007) 782–786.

[3] E. Collini, C. Y. Wong, K. E. Wilk, P. M. G. Curmi, P. Brumer and G. D. Scholes, Coherently wired light-harvesting in photosynthetic marine algae at ambient temperature, *Nature* **463** (2010) 644–647.

[4] D. B. Turner, R. Dinshaw, K.-K. Lee, M. S. Belsley, K. E. Wilk, P. M. G. Curmi and G. D. Scholes, Quantitative investigations of quantum coherence for a light-harvesting protein at conditions simulating photosynthesis, *Phys. Chem. Chem. Phys.* **14** (2012) 4857–4874.

[5] T. Scholak, F. Mintert, T. Wellens and A. Buchleitner, Quantum efficiency in complex systems, Part I: Biomolecular systems, in *Transport and Entanglement*, eds. E. R. Weber, M. Thorwart and U. Wrfel, Semiconductors and Semimetals, Vol. 83 (Academic Press, San Diego, 2010), pp. 1–38.
[6] T. Scholak, Transport and coherence in disordered networks, Dissertation, Albert-Ludwigs-Universität, Freiburg (2011).
[7] R. E. Fenna and B. W. Matthews, Chlorophyll arrangement in a bacteriochlorophyll protein from *chlorobium limicola*, *Nature* **258** (1975) 573–577.
[8] D. E. Tronrud, M. F. Schmid and B. W. Mathews, Structure and x-ray amino acid sequence of a bacteriochlorophyll a protein from *prosthecochloris aestuarii* refined at 1.9 Å resolution, *J. Mol. Biol.* **188** (1986) 444–453.
[9] D. E. Tronrud, J. Z. Wen, L. Gay and R. E. Blankenship, The structural basis for the difference in absorbance spectra for the FMO antenna protein from various green sulfur bacteria, *Photosynth. Res.* **100**(2) (2009) 79–87.
[10] R. Bümel, A. Buchleitner, R. Graham, L. Sirko, U. Smilansky and H. Walther, Dynamical localization in the microwave interaction of Rydberg atoms: The influence of noise, *Phys. Rev. A* **44** (1991) 4521–4540.
[11] V. Milner, D. A. Steck, W. H. Oskay and M. Raizen, Recovery of classically chaotic behavior in a noise-driven quantum system, *Phys. Rev. E* **61** (2000) 7223–7226.
[12] T. Scholak, T. Wellens and A. Buchleitner, The optimization topography of exciton transport, *Europhys. Lett.* **96**(1) (2011) 10001, doi:10.1209/0295-5075/96/10001.
[13] T. Scholak, F. de Melo, T. Wellens, F. Mintert and A. Buchleitner, Efficient and coherent excitation transfer across disordered molecular networks, *Phys. Rev. E* **83** (2011) 021912, 4 pp.
[14] A. Kay, Perfect state transfer: Beyond nearest-neighbor couplings, *Phys. Rev. A* **73** (2006) 032306.
[15] M.-H. Yung and S. Bose, Perfect state transfer, effective gates, and entanglement generation in engineered bosonic and fermionic networks, *Phys. Rev. A* **71** (2005) 032310, 6 pp.
[16] M. Walschaers, R. Mulet and A. Buchleitner, Optimally designed quantum transport across disordered networks, arXiv:1207.4072.
[17] T. Scholak, T. Wellens and A. Buchleitner, Optimal networks for excitonic energy transport, *J. Phys. B* **44** (2011) 184012, doi:10.1088/0953-4075/44/18/184012.
[18] T. Scholak, T. Wellens and A. Buchleitner, The optimization topography of exciton transport, *Europhys. Lett.* **96** (2011) 10001, doi:10.1209/0295-5075/96/10001.